DESY 95-081
hep-ex/9506001
May 1995

ISSN 0418-9833

The Gluon Density of the Proton at Low x from a QCD Analysis of F_2

H1 Collaboration

Abstract:

We present a QCD analysis of the proton structure function F_2 measured by the H1 experiment at HERA, combined with data from previous fixed target experiments. The gluon density is extracted from the scaling violations of F_2 in the range $2 \cdot 10^{-4} < x < 3 \cdot 10^{-2}$ and compared with an approximate solution of the QCD evolution equations. The gluon density is found to rise steeply with decreasing x.

S. Aid[13], V. Andreev[24], B. Andrieu[28], R.-D. Appuhn[11], M. Arpagaus[36], A. Babaev[26], J. Baehr[35], J. Bán[17], Y. Ban[27], P. Baranov[24], E. Barrelet[29], R. Barschke[11], W. Bartel[11], M. Barth[4], U. Bassler[29], H.P. Beck[37], H.-J. Behrend[11], A. Belousov[24], Ch. Berger[1], G. Bernardi[29], R. Bernet[36], G. Bertrand-Coremans[4], M. Besançon[9], R. Beyer[11], P. Biddulph[22], P. Bispham[22], J.C. Bizot[27], V. Blobel[13], K. Borras[8], F. Botterweck[4], V. Boudry[7], A. Braemer[14], F. Brasse[11], W. Braunschweig[1], V. Brisson[27], D. Bruncko[17], C. Brune[15], R.Buchholz[11], L. Büngener[13], J. Bürger[11], F.W. Büsser[13], A. Buniatian[11,38], S. Burke[18], M. Burton[22], G. Buschhorn[26], A.J. Campbell[11], T. Carli[26], F. Charles[11], M. Charlet[11], D. Clarke[5], A.B. Clegg[18], B. Clerbaux[4], M. Colombo[8], J.G. Contreras[8], C. Cormack[19], J.A. Coughlan[5], A. Courau[27], Ch. Coutures[9], G. Cozzika[9], L. Criegee[11], D.G. Cussans[5], J. Cvach[30], S. Dagoret[29], J.B. Dainton[19], W.D. Dau[16], K. Daum[34], M. David[9], B. Delcourt[27], L. Del Buono[29], A. De Roeck[11], E.A. De Wolf[4], P. Di Nezza[32], C. Dollfus[37], J.D. Dowell[3], H.B. Dreis[2], A. Droutskoi[23], J. Duboc[29], D. Düllmann[13], O. Dünger[13], H. Duhm[12], J. Ebert[34], T.R. Ebert[19], G. Eckerlin[11], V. Efremenko[23], S. Egli[37], H. Ehrlichmann[35], S. Eichenberger[37], R. Eichler[36], F. Eisele[14], E. Eisenhandler[20], R.J. Ellison[22], E. Elsen[11], M. Erdmann[14], W. Erdmann[36], E. Evrard[4], L. Favart[4], A. Fedotov[23], D. Feeken[13], R. Felst[11], J. Feltesse[9], J. Ferencei[15], F. Ferrarotto[32], K. Flamm[11], M. Fleischer[26], M. Flieser[26], G. Flügge[2], A. Fomenko[24], B. Fominykh[23], M. Forbush[7], J. Formánek[31], J.M. Foster[22], G. Franke[11], E. Fretwurst[12], E. Gabathuler[19], K. Gabathuler[33], K. Gamerdinger[26], J. Garvey[3], J. Gayler[11], M. Gebauer[8], A. Gellrich[11], H. Genzel[1], R. Gerhards[11], U. Goerlach[11], L. Goerlich[6], N. Gogitidze[24], M. Goldberg[29], D. Goldner[8], B. Gonzalez-Pineiro[29], I. Gorelov[23], P. Goritchev[23], C. Grab[36], H. Grässler[2], R. Grässler[2], T. Greenshaw[19], G. Grindhammer[26], A. Gruber[26], C. Gruber[16], J. Haack[35], D. Haidt[11], L. Hajduk[6], O. Hamon[29], M. Hampel[1], E.M. Hanlon[18], M. Hapke[11], W.J. Haynes[5], J. Heatherington[20], G. Heinzelmann[13], R.C.W. Henderson[18], H. Henschel[35], I. Herynek[30], M.F. Hess[26], W. Hildesheim[11], P. Hill[5], K.H. Hiller[35], C.D. Hilton[22], J. Hladký[30], K.C. Hoeger[22], M. Höppner[8], R. Horisberger[33], V.L. Hudgson[3], Ph. Huet[4], M. Hütte[8], H. Hufnagel[14], M. Ibbotson[22], H. Itterbeck[1], M.-A. Jabiol[9], A. Jacholkowska[27], C. Jacobsson[21], M. Jaffre[27], J. Janoth[15], T. Jansen[11], L. Jönsson[21], D.P. Johnson[4], L. Johnson[18], H. Jung[29], P.I.P. Kalmus[20], D. Kant[20], R. Kaschowitz[2], P. Kasselmann[12], U. Kathage[16], J. Katzy[14], H.H. Kaufmann[35], S. Kazarian[11], I.R. Kenyon[3], S. Kermiche[25], C. Keuker[1], C. Kiesling[26], M. Klein[35], C. Kleinwort[13], G. Knies[11], W. Ko[7], T. Köhler[1], J.H. Köhne[26], H. Kolanoski[8], F. Kole[7], S.D. Kolya[22], V. Korbel[11], M. Korn[8], P. Kostka[35], S.K. Kotelnikov[24], T. Krämerkämper[8], M.W. Krasny[6,29], H. Krehbiel[11], D. Krücker[2], U. Krüger[11], U. Krüner-Marquis[11], J.P. Kubenka[26], H. Küster[2], M. Kuhlen[26], T. Kurča[17], J. Kurzhöfer[8], B. Kuznik[34], D. Lacour[29], F. Lamarche[28], R. Lander[7], M.P.J. Landon[20], W. Lange[35], P. Lanius[26], J.-F. Laporte[9], A. Lebedev[24], C. Leverenz[11], S. Levonian[24], Ch. Ley[2], A. Lindner[8], G. Lindström[12], J. Link[7], F. Linsel[11], J. Lipinski[13], B. List[11], G. Lobo[27], P. Loch[27], H. Lohmander[21], J. Lomas[22], G.C. Lopez[20], V. Lubimov[23], D. Lüke[8,11], N. Magnussen[34], E. Malinovski[24], S. Mani[7], R. Maraček[17], P. Marage[4], J. Marks[25], R. Marshall[22], J. Martens[34], R. Martin[11], H.-U. Martyn[1], J. Martyniak[6], S. Masson[2], T. Mavroidis[20], S.J. Maxfield[19], S.J. McMahon[19], A. Mehta[22], K. Meier[15], D. Mercer[22], T. Merz[11], C.A. Meyer[37], H. Meyer[34], J. Meyer[11], A. Migliori[28], S. Mikocki[6], D. Milstead[19], F. Moreau[28], J.V. Morris[5], E. Mroczko[6], G. Müller[11], K. Müller[11], P. Murín[17], V. Nagovizin[23], R. Nahnhauer[35], B. Naroska[13], Th. Naumann[35], P.R. Newman[3], D. Newton[18], D. Neyret[29], H.K. Nguyen[29], T.C. Nicholls[3], F. Niebergall[13], C. Niebuhr[11], Ch. Niedzballa[1], R. Nisius[1], G. Nowak[6], G.W. Noyes[5], M. Nyberg-Werther[21], M. Oakden[19], H. Oberlack[26], U. Obrock[8], J.E. Olsson[11], D. Ozerov[23], E. Panaro[11], A. Panitch[4], C. Pascaud[27], G.D. Patel[19], E. Peppel[35], E. Perez[9], J.P. Phillips[22], Ch. Pichler[12], A. Pieuchot[25], D. Pitzl[36], G. Pope[7], S. Prell[11], R. Prosi[11], K. Rabbertz[1], G. Rädel[11], F. Raupach[1], P. Reimer[30], S. Reinshagen[11], P. Ribarics[26], H.Rick[8], V. Riech[12], J. Riedlberger[36], S. Riess[13], M. Rietz[2],

E. Rizvi[20], S.M. Robertson[3], P. Robmann[37], H.E. Roloff[35], R. Roosen[4], K. Rosenbauer[1]
A. Rostovtsev[23], F. Rouse[7], C. Royon[9], K. Rüter[26], S. Rusakov[24], K. Rybicki[6], R. Rylko[20],
N. Sahlmann[2], E. Sanchez[26], D.P.C. Sankey[5], P. Schacht[26], S. Schiek[11], P. Schleper[14], W. von Schlippe[20],
C. Schmidt[11], D. Schmidt[34], G. Schmidt[13], A. Schöning[11], V. Schröder[11], E. Schuhmann[26],
B. Schwab[14], A. Schwind[35], F. Sefkow[11], M. Seidel[12], R. Sell[11], A. Semenov[23], V. Shekelyan[11],
I. Sheviakov[24], H. Shooshtari[26], L.N. Shtarkov[24], G. Siegmon[16], U. Siewert[16], Y. Sirois[28],
I.O. Skillicorn[10], P. Smirnov[24], J.R. Smith[7], V. Solochenko[23], Y. Soloviev[24], J. Spiekermann[8],
S. Spielman[28], H. Spitzer[13], R. Starosta[1], M. Steenbock[13], P. Steffen[11], R. Steinberg[2], B. Stella[32],
K. Stephens[22], J. Stier[11], J. Stiewe[15], U. Stösslein[35], K. Stolze[35], J. Strachota[30], U. Straumann[37],
W. Struczinski[2], J.P. Sutton[3], S. Tapprogge[15], V. Tchernyshov[23], C. Thiebaux[28], G. Thompson[20],
P. Truöl[37], J. Turnau[6], J. Tutas[14], P. Uelkes[2], A. Usik[24], S. Valkár[31], A. Valkárová[31],
C. Vallée[25], P. Van Esch[4], P. Van Mechelen[4], A. Vartapetian[11,38], Y. Vazdik[24], P. Verrecchia[9],
G. Villet[9], K. Wacker[8], A. Wagener[2], M. Wagener[33], I.W. Walker[18], A. Walther[8], G. Weber[13],
M. Weber[11], D. Wegener[8], A. Wegner[11], H.P. Wellisch[26], L.R. West[3], S. Willard[7], M. Winde[35],
G.-G. Winter[11], C. Wittek[13], A.E. Wright[22], E. Wünsch[11], N. Wulff[11], T.P. Yiou[29], J. Žáček[31],
D. Zarbock[12], Z. Zhang[27], A. Zhokin[23], M. Zimmer[11], W. Zimmermann[11], F. Zomer[27], and
K. Zuber[15]

[1] I. Physikalisches Institut der RWTH, Aachen, Germany[a]
[2] III. Physikalisches Institut der RWTH, Aachen, Germany[a]
[3] School of Physics and Space Research, University of Birmingham, Birmingham, UK[b]
[4] Inter-University Institute for High Energies ULB-VUB, Brussels; Universitaire Instelling Antwerpen, Wilrijk, Belgium[c]
[5] Rutherford Appleton Laboratory, Chilton, Didcot, UK[b]
[6] Institute for Nuclear Physics, Cracow, Poland[d]
[7] Physics Department and IIRPA, University of California, Davis, California, USA[e]
[8] Institut für Physik, Universität Dortmund, Dortmund, Germany[a]
[9] CEA, DSM/DAPNIA, CE-Saclay, Gif-sur-Yvette, France
[10] Department of Physics and Astronomy, University of Glasgow, Glasgow, UK[b]
[11] DESY, Hamburg, Germany[a]
[12] I. Institut für Experimentalphysik, Universität Hamburg, Hamburg, Germany[a]
[13] II. Institut für Experimentalphysik, Universität Hamburg, Hamburg, Germany[a]
[14] Physikalisches Institut, Universität Heidelberg, Heidelberg, Germany[a]
[15] Institut für Hochenergiephysik, Universität Heidelberg, Heidelberg, Germany[a]
[16] Institut für Reine und Angewandte Kernphysik, Universität Kiel, Kiel, Germany[a]
[17] Institute of Experimental Physics, Slovak Academy of Sciences, Košice, Slovak Republic[f]
[18] School of Physics and Materials, University of Lancaster, Lancaster, UK[b]
[19] Department of Physics, University of Liverpool, Liverpool, UK[b]
[20] Queen Mary and Westfield College, London, UK[b]
[21] Physics Department, University of Lund, Lund, Sweden[g]
[22] Physics Department, University of Manchester, Manchester, UK[b]
[23] Institute for Theoretical and Experimental Physics, Moscow, Russia
[24] Lebedev Physical Institute, Moscow, Russia[f]
[25] CPPM, Université d'Aix-Marseille II, IN2P3-CNRS, Marseille, France
[26] Max-Planck-Institut für Physik, München, Germany[a]
[27] LAL, Université de Paris-Sud, IN2P3-CNRS, Orsay, France
[28] LPNHE, Ecole Polytechnique, IN2P3-CNRS, Palaiseau, France
[29] LPNHE, Universités Paris VI and VII, IN2P3-CNRS, Paris, France
[30] Institute of Physics, Czech Academy of Sciences, Praha, Czech Republic[f,h]

[31] Nuclear Center, Charles University, Praha, Czech Republic[f,h]
[32] INFN Roma and Dipartimento di Fisica, Universita "La Sapienza", Roma, Italy
[33] Paul Scherrer Institut, Villigen, Switzerland
[34] Fachbereich Physik, Bergische Universität Gesamthochschule Wuppertal, Wuppertal, Germany[a]
[35] DESY, Institut für Hochenergiephysik, Zeuthen, Germany[a]
[36] Institut für Teilchenphysik, ETH, Zürich, Switzerland[i]
[37] Physik-Institut der Universität Zürich, Zürich, Switzerland[i]
[38] Visitor from Yerevan Phys.Inst., Armenia

[a] Supported by the Bundesministerium für Forschung und Technologie, FRG under contract numbers 6AC17P, 6AC47P, 6DO57I, 6HH17P, 6HH27I, 6HD17I, 6HD27I, 6KI17P, 6MP17I, and 6WT87P
[b] Supported by the UK Particle Physics and Astronomy Research Council, and formerly by the UK Science and Engineering Research Council
[c] Supported by FNRS-NFWO, IISN-IIKW
[d] Supported by the Polish State Committee for Scientific Research, grant No. 204209101
[e] Supported in part by USDOE grant DE F603 91ER40674
[f] Supported by the Deutsche Forschungsgemeinschaft
[g] Supported by the Swedish Natural Science Research Council
[h] Supported by GA ČR, grant no. 202/93/2423 and by GA AV ČR, grant no. 19095
[i] Supported by the Swiss National Science Foundation

1 Introduction

The study of scaling violations of the proton structure function is a traditional method to obtain information on the gluon density inside the proton [1, 2]. New structure function measurements made at the electron-proton collider HERA at a center of mass energy of 296 GeV open a completely new kinematic region for this study. The accessible range in the Bjorken-scaling variable x has been extended down to about 10^{-4}, two orders of magnitude lower than previous fixed target experiments. To know the gluon density in this region is particularly interesting since here gluons are expected to dominate the proton structure. Studies of parton densities can provide a sensitive test of perturbative QCD in the small x region and can reveal the onset of new effects, such as parton density saturation in the proton. The gluon density or, more generally, the parton densities inside the proton must be known in order to determine the production rates of hadronic processes which can be described by perturbative QCD. At future high energy hadron colliders such processes involve parton densities at x values below 10^{-3}.

The H1 collaboration recently published a measurement of the proton structure function $F_2(x, Q^2)$ [3] derived from ep scattering data taken in 1993 corresponding to a luminosity of 271 nb^{-1}. This measurement confirmed with improved significance the observation made already in 1992 by H1 [4] and ZEUS [5] that the structure function exhibits a strong rise towards low x. This rise has caused much debate as to whether it results from conventional DGLAP QCD evolution [6] of the parton densities, or whether a new regime is entered where the dynamics is described by the BFKL evolution equation [7]. The latter QCD evolution equation is expected to be particularly suited for the study of the small x region since it resums all leading $\log(1/x)$ terms in the perturbative expansion.

Using global fit methods, it will be shown that the measured proton structure function F_2 can be well described by the DGLAP evolution equations in this new kinematic domain. Then the DGLAP equations are used to extract the gluon density in the proton. Taking into account all systematic errors of the H1 F_2 measurement and their correlations a full error analysis of the gluon density is performed. A similar analysis was recently made by the ZEUS collaboration [8]. A hybrid fit using the BFKL equation for the evolution of the gluon density at small x and DGLAP equations elsewhere is also attempted and is found to describe the data equally well.

Besides these global fit techniques, two approximate methods are discussed which relate the partonic densities at a given x value to the local scaling violation in that region. Finally, following the method described in [9] the F_2 data is studied in the context of double asymptotic scaling, showing that they can be described within this framework.

This paper concentrates on the QCD analysis of the F_2 measurement of H1. For a description of the analysis leading to this measurement see to [3]. The H1 detector is described in [10].

2 Global QCD Fits

2.1 Fits with the DGLAP Evolution Equations

The DGLAP evolution equations are solved numerically in the next-to-leading $\log(Q^2)$ and leading $\log(Q^2)$ approximation. Two independent programs based on the methods of [13] and

[14] were used and were checked to give the same results at the percent level. For the next-to-leading $\log(Q^2)$ approximation the splitting functions [11] and the strong coupling constant $\alpha_s(Q^2)$ are defined in the $\overline{MS}$ factorization and renormalization schemes [12]. Starting from $Q_0^2 = 4$ GeV^2, the gluon density g and the non-singlet and singlet quark densities q_{NS} and q_{SI} are evolved to higher Q^2 values. The singlet quark density is defined as $q_{SI} = u+\bar{u}+d+\bar{d}+s+\bar{s}$. The non-singlet quark density is given by $q_{NS} = u + \bar{u} - q_{SI}/3$. The following functional forms are assumed at Q_0^2 :

$$\begin{aligned} xg(x) &= A_g x^{B_g}(1-x)^{C_g} \\ xq_{NS}(x) &= A_{NS} x^{B_{NS}}(1-x)^{C_{NS}}(1+D_{NS}x) \\ xq_{SI}(x) &= A_{SI} x^{B_{SI}}(1-x)^{C_{SI}}(1+D_{SI}x). \end{aligned} \tag{1}$$

Only proton data is used in the fit. In order to constrain the singlet contribution without including isoscalar target data we impose the momentum fraction carried by the gluon to be 0.44 [2] at $Q_0^2 = 4$ GeV^2. The normalization parameter A_{SI} of the quark density is then constrained by imposing the momentum sum rule: $\int_0^1 [xg(x) + xq_{SI}(x)]dx = 1$. The shape of the gluon distribution changes only very weakly if the momentum fraction carried by the gluons is varied within 6%, which corresponds to three times its error given in [2]. In the DGLAP evolution equations only three active light quark flavours are taken into account. Heavy quark contributions are dynamically generated using the photon-gluon fusion prescription given in [17, 18], extended to next-to-leading order according to [19] and the charm mass is assumed to be $m_c = 1.5$ GeV. In this approach the contribution of beauty quarks remains small and can be neglected. The QCD mass scale parameter $\Lambda^{(4)}_{\overline{MS}}$ for four flavours is kept as a free parameter in the fit. Continuity of $\alpha_s(Q^2)$ is imposed at the charm and beauty quark mass thresholds using the prescription in [15]. The small x behaviour of the gluon and the singlet quark densities are kept independent, similar to the procedure recently advocated in [16]. The structure function $F_2(x, Q^2)$ is obtained by convoluting the evolved parton densities with the Wilson coefficients [12].

In [20] it was shown that about 10% of the events are diffractive events, i.e. the electron scatters on a component of the proton which is not colour connected with the rest of the proton. At this stage there is no experimental evidence that the QCD evolution of the diffractive part of F_2 is significantly different from that of the total inclusive F_2. Furthermore, these contributions are most likely also present in the lower energy data and were not subtracted there either. Hence these events are kept in the data allowing a comparison with results from other analyses.

2.2 Fits with the Mixed DGLAP-BFKL Evolution Equations

The BFKL equation accounts for the leading $\log(1/x)$ terms in the perturbative expansion, which dominate in the limit of small x. Since it only describes the evolution of the gluon density a prescription [21] is needed to determine F_2. Here, the method detailed in [22] is used. The $x - Q^2$ plane is divided into two regions : for $x > x_0$ the conventional leading $\log(Q^2)$ DGLAP equations are used, while for $x < x_0$ the gluon density is extracted applying the BFKL evolution equation. In the latter low x region, the singlet quark density is computed using the leading $\log(Q^2)$ DGLAP equation, but including the results of the evolved low x gluon distribution. The transition point x_0 is left as a free parameter in the fit. Since the

BFKL equation is an evolution equation in $\log(1/x)$, an input gluon density is required at the transition point x_0 for all Q^2 values. This is obtained by requiring continuity of the gluon density and of its $\log(Q^2)$ derivative at x_0. The continuity of all parton densities is preserved by taking the same input functions (eq. 1) at Q_0^2 to solve the DGLAP equations in both regions. For the starting gluon density at a low $Q^2 \lesssim 1$ GeV^2 in the non-perturbative region the prescription of [23] is used : $\partial x g(x,Q^2)/\partial \log(Q^2) \sim Q^2/(Q^2+k_a^2)$ where k_a^2 is a free parameter. The heavy quark contribution is treated in the same way as for the full DGLAP fit.

Based on this procedure a leading $\log(Q^2)$ fit program [14] has been written. In order to stay in the region where $\log(1/x)$ dominates over $\log(Q^2)$ only data with $Q^2 \leq 50$ GeV^2 are used for this study. The best fit yields a value of $x_0 = 10^{-2}$.

2.3 Results of the Global Fits

The structure function data reported by the H1 experiment cover a large span in x, reaching values down to $2 \cdot 10^{-4}$, but do not cover the high x region. In order to constrain the structure function at high x data from the fixed target muon-hydrogen scattering experiments NMC [24] and BCDMS [25] are used. The parton densities are fitted with the evolution equations to the F_2 data, taking into account statistical errors only to calculate the χ^2. The normalization of each experiment is left free within the limits of their quoted errors (H1: 4.5%, NMC(90): 1.6%, NMC(280): 2.6%, BCDMS: 3%) [3, 24, 25], leading to four additional fit parameters [26]. To avoid regions where target corrections and higher twist effects [27] could become important data from the fixed target experiments in the ranges $Q^2 < 4$ GeV$^2, x < 0.5$ and $Q^2 < 15$ GeV$^2, x \geq 0.5$ were not included in the fit. The χ^2 was minimized using the MINUIT program [28].

The results on the fit parameters are shown in Tab. 1 and 2. The contributions to the total χ^2 from the different experiments are also given. We obtained $\Lambda^{(4)}_{\overline{MS}} = 225$ MeV, a value compatible with those found by dedicated analyses [29]. Since the aim of this analysis is to extract the gluon density, emphasis has been put on the treatment of the errors on the gluon density rather than on the fit parameters. Fig. 1 shows the result of the next-to-leading $\log(Q^2)$ QCD fit together with F_2 data points as a function of x. Unlike this analysis and the analysis in [16] the parameters B_{SI} and B_g were frequently taken to be equal [30, 31], motivated by the expectation that there is a strong coupling between the sea quark densities and the gluon density. Therefore another fit was performed requiring $B_g = B_{SI} = B$, resulting in a value of $B = -0.14$ and a χ^2 increased by 3 units. This increase stems mainly from the lowest x bin F_2 measurement (Fig. 2) where the $\log(Q^2)$ slope is flatter than expected by the DGLAP evolution.

Fig. 2 presents the results from fits using the leading $\log(Q^2)$ DGLAP equations and the mixed DGLAP-BFKL equations, together with the F_2 measurements. Both the DGLAP and the mixed DGLAP-BFKL results give a good description of the Q^2 evolution of the structure function. The χ^2 of the DGLAP fit is 557. Small differences between the two fits occur at the lowest x bin which result in a gain in χ^2 of 7 units in favour of the mixed DGLAP-BFKL fit. Thus both approaches describe the data with equal quality. Higher precision and measurements at lower values of x and Q^2 expected from future HERA data may allow to discriminate between the approaches.

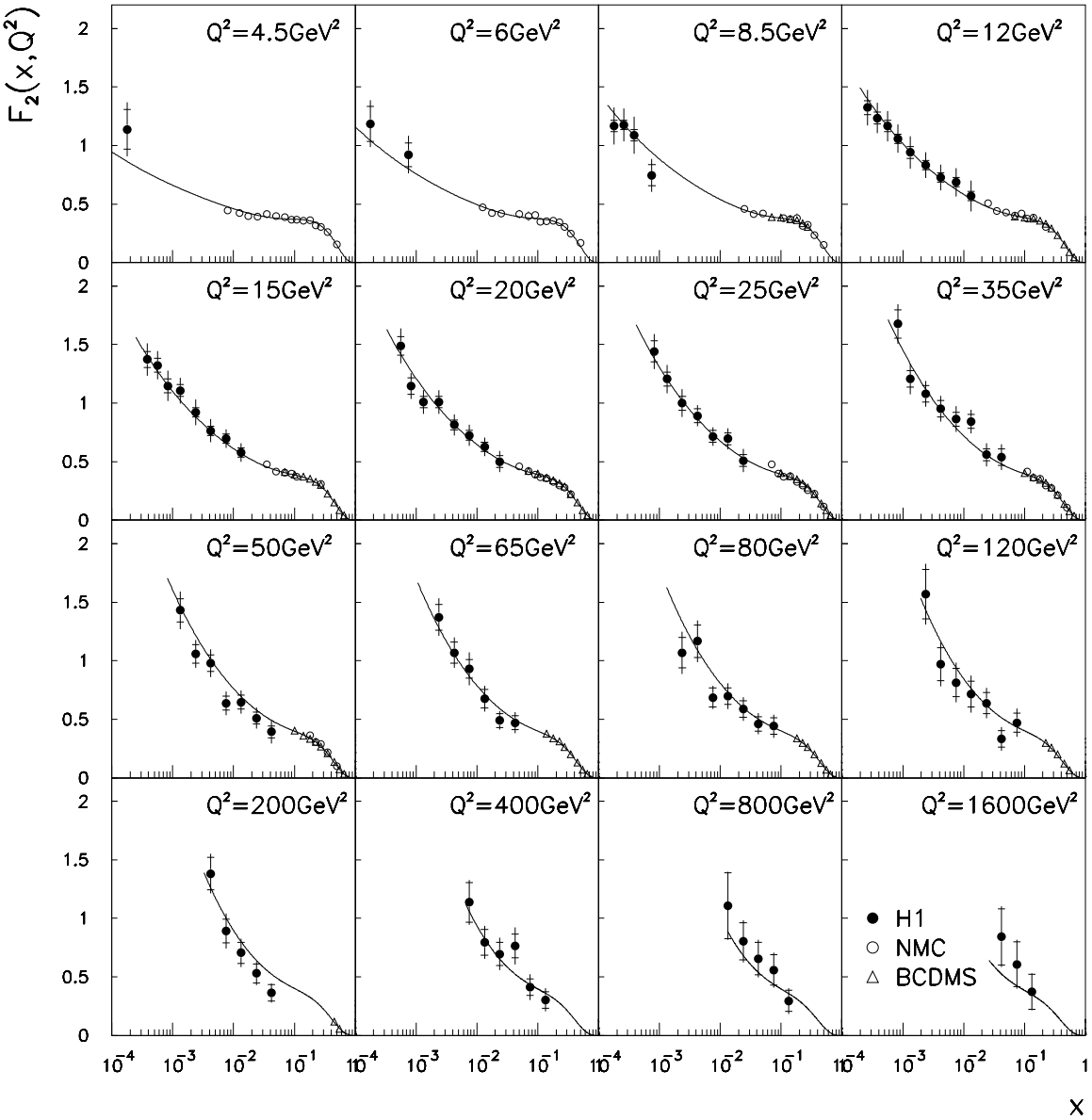

Figure 1: $F_2(x, Q^2)$ measured by H1 together with NMC and BCDMS fixed target results. The inner error bar is the statistical error. The full error represents the statistical and systematic errors added in quadrature, not taking into account the normalization uncertainties (see text). The full line represents the next-to-leading $\log(Q^2)$ DGLAP fit.

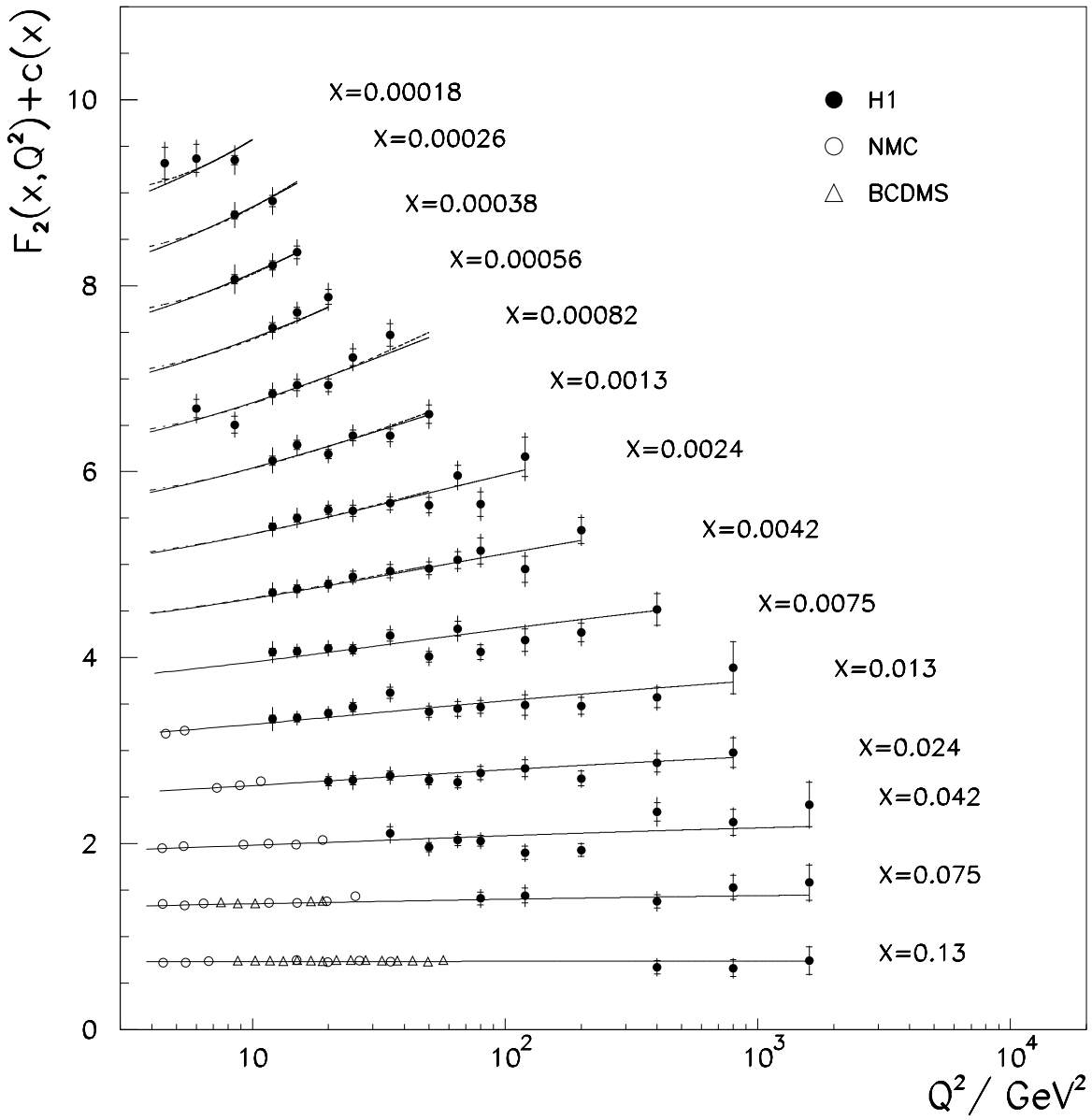

Figure 2: $F_2(x, Q^2)$ measured by H1 together with NMC and BCDMS fixed target results. The full and dashed lines represent the leading $\log(Q^2)$ DGLAP and mixed DGLAP-BFKL fits. The F_2 values are plotted with a binning constant $c(x) = 0.6(i - 0.4)$ where i is the x bin number starting from $x = 0.13$. The inner error bar is the statistical error. The full error represents the statistical and systematic errors added in quadrature, not taking into account the normalization uncertainties (see text).

parameter	A_g	B_g	C_g	A_{SI}	B_{SI}	C_{SI}	D_{SI}	A_{NS}	B_{NS}	C_{NS}	D_{NS}
	1.86	-0.22	7.12	1.15	-0.11	3.10	3.12	1.14	0.65	4.66	8.68

Table 1: Parameters of the next-to-leading $\log(Q^2)$ DGLAP fit.

Experiment	H1	NMC 90	NMC 280	BCDMS	total
data points	93	34	53	174	354
χ^2	129	55	127	192	509
normalization	0.93	1.00	1.01	0.97	

Table 2: The number of data points, the χ^2 and the normalization factors for each experiment.

Fig. 3a shows the gluon density $xg(x)$ at $Q^2 = 20$ GeV^2, extracted with the next-to-leading $\log(Q^2)$ DGLAP evolution equations. A strong rise of the gluon density towards low x is observed. If this rise continues with decreasing x, the gluons are expected to fill up the transverse size of the proton. A naive calculation on the limit where a uniform gluon density fills the proton [32] leads to $xg(x) \simeq 6Q^2$, Q^2 in GeV^2. Hence the gluon density determined at $Q^2 = 20$ GeV^2 and $x = 2 \cdot 10^{-4}$ is still well below this limit. The statistical error band of the fitted gluon results from a fit considering the statistical errors of the data points only.

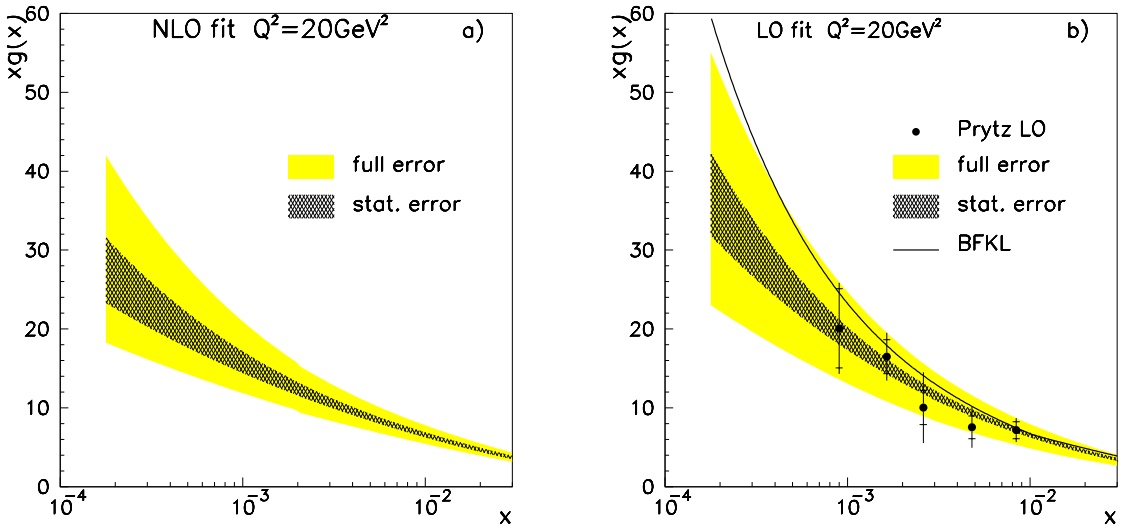

Figure 3: a) The gluon density $xg(x)$ at $Q^2 = 20$ GeV^2 extracted from a next-to-leading $\log(Q^2)$ QCD fit. The procedure to derive the error bands is described in the text. b) The gluon density $xg(x)$ at $Q^2 = 20$ GeV^2 from a leading $\log(Q^2)$ QCD fit (shaded) and a mixed DGLAP-BFKL fit (full line). The points are calculated using the method of Prytz. The inner error bars represent the statistical errors. The outer error bars are the statistical and systematic errors added in quadrature.

In [3] a full account is given of the systematic errors on the F_2 of H1. These errors cannot be translated simply into an error on the gluon density, since they are often strongly correlated from point to point. A careful study of how each individual error source affects the measured F_2 points has been made. For example, the way in which calibration uncertainties influence the F_2 measurement depends on the method used to reconstruct the kinematics. From this

study, a total of 26 independent systematic error contributions has been established, which cause shifts to the F_2 points. In order to properly account for the point to point correlations a new fit parameter was introduced for each systematic error source. The χ^2 covariance matrix and the Lagrange multiplier method [33] were used to calculate the error band of the gluon density shown in Fig. 3.

To evaluate the effect of Λ on the gluon density two fits have been performed, fixing $\Lambda^{(4)}_{\overline{MS}} = 180$ MeV and $\Lambda^{(4)}_{\overline{MS}} = 280$ MeV in order to cover the span of values quoted in [29]. Further the momentum fraction carried by the gluons is varied between 0.38 and 0.50. The systematic shifts between the extracted gluon densities with different $\Lambda^{(4)}$ and gluon momentum fraction values are added quadratically to the systematic uncertainty. It does not significantly affect the total error of the gluon density in the small x region. The effect of the charm mass, which enters the calculation via the photon-gluon fusion processes has been studied, by varying m_c between 1 GeV and 2 GeV. This changes the resulting gluon density inside the statistical error band only. In the same way, the photon-gluon fusion energy scale was changed from $2m_c$ to $\sqrt{m_c^2 + Q^2}$. The resulting variation of the gluon density was found to be inside the statistical error band. The full systematic error band of the gluon density is shown in Fig. 3.

In Fig. 3b the gluon density resulting from a leading $\log(Q^2)$ fit of the DGLAP equations to the H1, NMC and BCDMS data is shown. The error bands are calculated as detailed above. The gluon density is higher compared to the next-to-leading $\log(Q^2)$ fit result. The value for the exponent in the gluon density B_g is -0.32 ($A_g = 1.17$; $C_g = 5.51$), and the value for $\Lambda^{(4)}_{\rm LO}$ amounts to 185 MeV. The result of the mixed DGLAP-BFKL fit is also shown.

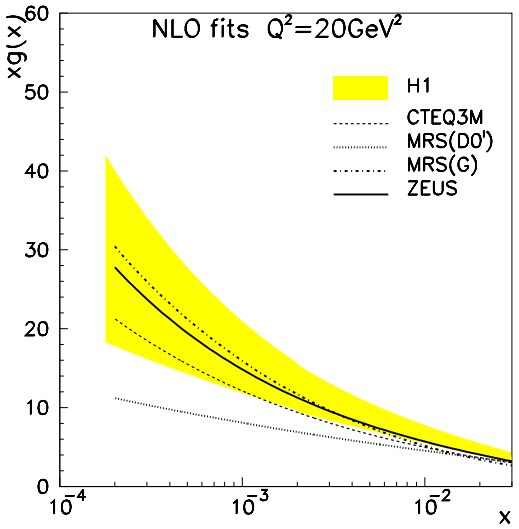

Figure 4: The gluon density $xg(x)$ at $Q^2 = 20$ GeV^2 extracted from a next-to-leading $\log(Q^2)$ QCD fit as in Fig. 3a together with the ZEUS fit [8] and the parametrizations CTEQ3M, MRSD0' and MRSG.

Fig. 4 shows once more the gluon density as extracted by H1 from the next-to-leading $\log(Q^2)$ QCD fit together with the ZEUS fit result [8] and the parametrizations of CTEQ3M [30], MRSD0' [31] and MRSG [16]. The H1 measurement clearly disfavours the MRSD0' parametrization. The ZEUS result and the CTEQ3M and MRSG parametrizations show a steep rise of the gluon distribution towards small x as well. Differences of the H1 analysis with these results

x	$\frac{\partial F_2}{\partial \log(Q^2)}$	σ_{stat}	σ_{syst}	$\frac{\partial \log(F_2)}{\partial \log(Q^2)}$	σ_{stat}	σ_{syst}	$\frac{Q^2}{\mathrm{GeV}^2}$	$\frac{\partial \log(F_2)}{\partial \log(1/x)}$	σ_{stat}	σ_{syst}
0.000383	0.51	0.14	0.09	0.41	0.11	0.09	8.5	0.19	0.07	0.06
0.000562	0.65	0.18	0.10	0.47	0.13	0.09	12	0.21	0.02	0.08
0.000825	0.46	0.06	0.06	0.41	0.05	0.05	15	0.25	0.02	0.07
0.001330	0.28	0.06	0.11	0.24	0.05	0.08	20	0.25	0.02	0.05
0.002370	0.21	0.03	0.06	0.21	0.03	0.05	25	0.28	0.02	0.07
0.004210	0.20	0.03	0.03	0.21	0.03	0.04	35	0.26	0.02	0.06
0.007500	0.08	0.02	0.03	0.11	0.03	0.03	50	0.36	0.03	0.10
0.013300	0.06	0.02	0.02	0.08	0.03	0.03	65	0.40	0.04	0.10

Table 3: The logarithmic derivatives $\partial F_2(x,Q^2)/\partial \log(Q^2)$ and $\partial \log(F_2(x,Q^2))/\partial \log(Q^2)$ for different values of x (left), and the logarithmic derivatives $\partial \log(F_2(x,Q^2))/\partial log(1/x)$ for different values of Q^2 (right) with statistical and systematic errors.

are due to different data sets used in the gluon extraction, different starting parametrizations, a different data normalization procedure and to a smaller extent to the different scheme used for generating heavy flavour contributions.

3 Extraction of the Gluon Density from $\partial F_2(x,Q^2)/\partial \log Q^2$

In this section two recently proposed approximate methods which reduce the coupled integro-differential DGLAP equations to simple differential equations in $\log(Q^2)$ are discussed. The idea is to use the logarithmic derivatives of $F_2(x,Q^2)$ locally in x and Q^2 to approximately derive the gluon density.

In Tab. 3 the logarithmic derivatives $\partial F_2(x,Q^2)/\partial \log(Q^2)$ and $\partial \log F_2(x,Q^2)/\partial \log(Q^2)$ are given for different x values, determined from straight line fits to the H1 data. These quantities are advocated to be useful for QCD studies with approximate methods. This usage of a straight line fit is correct to within 10% at 20 GeV^2, as derived from the phenomenological F_2 parametrization of H1 presented in [3]. In order to determine the systematic errors on these values the following procedure was followed. All systematic errors discussed in [3] were used in turn to calculate a new set of F_2 values, and new derivatives were determined by fitting each of these new sets of shifted F_2 values. The differences of the new derivatives with the unshifted values were added quadratically to calculate the total systematic error.

The first approximate method used was suggested by Prytz [34]. To extract the gluon density in leading $\log(Q^2)$ he exploited the fact that at low x the scaling violations of F_2 arise mainly from pair creation of quarks from gluons. The approximation was later extended by the author to next-to-leading $\log(Q^2)$ [35]. Here only the leading $\log(Q^2)$ approximation is shown since it is extremely simple. The assumption to neglect the quark contribution leads to the following relation:

$$\frac{\partial F_2(x/2,Q^2)}{\partial \log(Q^2)} = \frac{10}{27}\frac{\alpha_s(Q^2)}{\pi} \cdot xg(x). \qquad (2)$$

The result is shown in Fig. 3b together with the leading $\log(Q^2)$ fit result. The value $\Lambda =$ 185 MeV from the fit was used as input for the Prytz approximation. A variation of Λ by

± 80 MeV changes the result of the approximation by about 10%. Depending on the steepness of the gluon density for $Q^2 = 20$ GeV^2 and $10^{-4} < x < 10^{-2}$ the theoretical correction to the Prytz approximation could rise up to –20%, about half of which comes from the neglect of the quark densities. In all, the gluon density given by the leading $\log(Q^2)$ fit and by the approximate method agree within the expected precision and both show the rise of $xg(x)$ at small x.

Another method was suggested by Ellis, Kunszt and Levin[36] who, inspired by the BFKL equation, assume the following shape for the gluon and quark-singlet distributions: $xg(x) = A_g x^{-\omega_0}$ and $xq_{SI}(x) = A_{SI} x^{-\omega_0}$. A prescription is given to extract the gluon density from the measured quantities $F_2(x,Q^2)$, $\partial F_2(x,Q^2)/\partial \log(Q^2)$ and $\omega_0 = \partial \log F_2(x,Q^2)/\partial \log(1/x)$. The slopes ω_0 are determined by fitting $\log F_2$ as a function of $\log(1/x)$. The result is shown in Tab. 3: F_2 becomes steeper in $(1/x)$ with increasing Q^2. The systematic and statistical errors on the derivatives were determined in the same way as for the $\partial F_2(x,Q^2)/\partial \log(Q^2)$ analysis. For $10 < Q^2 < 50$ GeV^2 we find $\omega_0 \approx 0.25$. According to [36], for $\omega_0 = 0.25$ the approximation can only be applied for $x < 3 \cdot 10^{-4}$. Since this is essentially outside the H1 measurement region, this method to extract the gluon density is not applied.

4 Double Asymptotic Scaling

Based on earlier QCD studies [37] Ball and Forte [9] show that evolving a flat input distribution at $Q_0^2 = 1$ GeV^2 with the DGLAP equations leads to a strong rise of F_2 at low x in the region measured by HERA. An interesting feature is that if QCD evolution is the underlying dynamics of the rise, perturbative QCD predicts that at large Q^2 and small x the structure function exhibits double scaling in the two variables:

$$\sigma \equiv \sqrt{\log(x_0/x) \cdot \log(t/t_0)}, \quad \rho \equiv \sqrt{\frac{\log(x_0/x)}{\log(t/t_0)}} \tag{3}$$

with $t \equiv \log(Q^2/\Lambda^2)$.

This follows from a computation [37] of the asymptotic form of the structure function $F_2(x,Q^2)$ at small x and relies only on the assumption that any increase in $F_2(x,Q^2)$ at small x is generated by perturbative QCD evolution. The asymptotic behaviour of $F_2(\sigma,\rho)$ is then:

$$F_2(\sigma,\rho) \sim f(\frac{\gamma}{\rho}) \frac{\gamma}{\rho} \frac{1}{\sqrt{\gamma\rho}} \exp\left[2\gamma\sigma - \delta\frac{\sigma}{\rho}\right] \times \left[1 + \mathcal{O}(\frac{1}{\sigma})\right]. \tag{4}$$

Here $\gamma \equiv 2\sqrt{3/b_0}$ with b_0 being the leading order coefficient of the β function of the QCD renormalization group equation for four flavours, $\delta = 1.36$ for four flavours and three colours. The function f depends on details of the starting distribution and tends to one in the asymptotic limit.

In order to test this prediction H1 data are presented in the variables σ and ρ, taking the boundary conditions to be $x_0 = 0.1$ and $Q_0^2 = 1$ GeV^2, and $\Lambda^{(4)}_{\rm LO} = 185$ MeV. The measured values of F_2 are rescaled by

$$R'_F(\sigma,\rho) = 8.1 \exp\left(\delta\frac{\sigma}{\rho} + \frac{1}{2}\log(\sigma) + \log(\frac{\rho}{\gamma})\right), \tag{5}$$

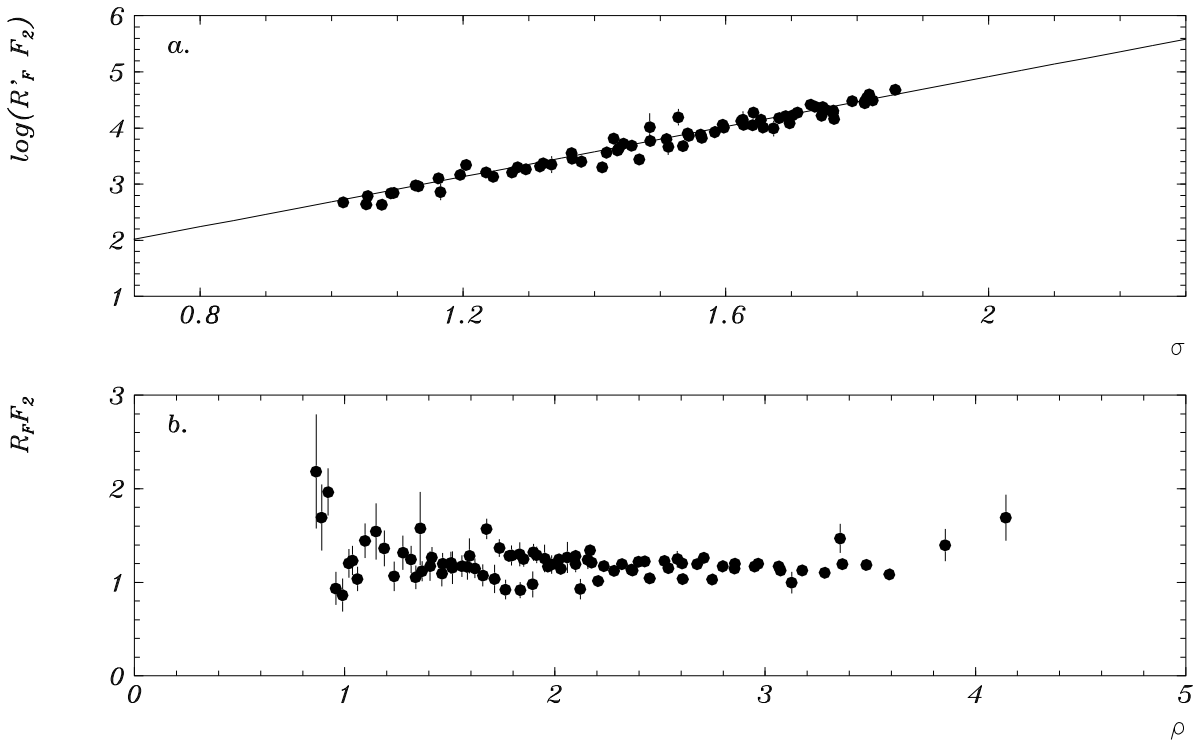

Figure 5: The rescaled structure functions $\log(R'_F F_2)$ and $R_F F_2$ plotted versus the variables σ and ρ defined in the text. Only data with $\rho^2 > 1.5$ are shown in a.

to remove the part of the leading subasymptotic behaviour which can be calculated in a model independent way; $\log(R'_F F_2)$ is then predicted to rise linearly with σ.

Fig. 5a shows that indeed the H1 data show a linear rise. A fit to the data gives a value of $2.22 \pm 0.04 \pm 0.10$ for the slope, the first error being statistical and the second systematic. The latter was obtained in the same way as discussed in section 3. Varying Λ by 80 MeV leads to an additional systematic uncertainty of 10%. The result agrees well with the prediction for the slope of $2\gamma = 2.4$, which is expected to become smaller by taking into account higher order corrections [38]. Fig. 5a contains only data with $\rho^2 > 1.5$, for which it is shown below that ρ is in the asymptotic region.

Scaling in ρ can be shown by multiplying F_2 by the factor $R_F \equiv R'_F e^{-2\gamma\sigma}$ removing all the leading behaviour in eq. 4. This rescaled structure function should scale in both σ and ρ when both lie in the asymptotic region: $R_F F_2 = N + \mathcal{O}(1/\sigma) + \mathcal{O}(1/\rho)$. While the scaling in σ can be deduced from Fig. 5a, we show the scaling in ρ in Fig. 5b. Scaling sets on for $\rho \gtrsim 1.2$ which determined the cut of $\rho^2 > 1.5$ for Fig. 5a.

The prediction for $R_F F_2$ as a function of ρ only depends on the gluon density at Q_0^2. While for a soft starting gluon distribution scaling for the full asymptotic region is predicted, a hard gluon input would lead to scaling violations at high ρ [9]. The data shown in Fig. 5 are well described by the asymptotic behaviour derived from soft boundary conditions, although within the present precision of the data a moderate increase at high ρ is not excluded. In addition the inclusion of higher order corrections is expected to give a similar rise at high ρ [38].

5 Summary

QCD fits were performed on the measured H1 proton structure function combined with NMC and BCDMS data using both the pure DGLAP and mixed DGLAP-BFKL evolution schemes in the range $Q^2 > 4$ GeV^2 and $2 \cdot 10^{-4} < x < 3 \cdot 10^{-2}$. Both prescriptions give a good description of the data. The data do not extend to low enough x or have sufficient precision for it to be possible to discriminate between the two approaches. Leading $\log(Q^2)$ and next-to-leading $\log(Q^2)$ fits are made to the data with comparable quality.

The gluon density is extracted in this region with a full error analysis including all systematic errors. It is found to rise steeply with decreasing x. An approximation of Prytz for the extraction of the gluon density agrees with the QCD fit within its expected precision. Double asymptotic scaling is observed in the region of our data.

Acknowledgements

We are grateful to the HERA machine group whose outstanding efforts made the structure function measurement possible. We appreciate the immense effort of the engineers and technicians who constructed and maintained the detector. We thank the funding agencies for their financial support of the experiment. We wish to thank the DESY directorate for the support and hospitality extended to the non-DESY members of the collaboration. We thank S.Riemersma for providing the code for the next-to-leading order photon-gluon fusion model and useful discussions. We also would like to thank J. Kwieciński, A. Vogt, A. Martin, R. Roberts, and J. Stirling for helpful discussions.

References

[1] A.C. Benvenuti et al., Phys. Lett. B223 (1989) 490.

[2] M. Arneodo et al., Phys. Lett. B309 (1993) 222.

[3] T. Ahmed et al., H1 Collaboration, Nucl. Phys. B439 (1995) 471.

[4] I. Abt et al., H1 Collaboration, Nucl. Phys. B407 (1993) 515.

[5] M. Derrick et al., ZEUS Collaboration, Phys. Lett. B316 (1993) 412.

[6] V.N. Gribov and L.N. Lipatov, Sov. Journ. Nucl. Phys. 15 (1972) 438 and 675;
G. Altarelli and G. Parisi, Nucl. Phys. B126 (1977) 298;
Yu.L. Dokshitzer, Sov. Phys. JETP 46 (1977) 641.

[7] E.A. Kuraev, L.N. Lipatov and V.S. Fadin, Sov. Phys. JETP 45 (1977) 199;
Y.Y. Balitsky and L.N. Lipatov, Sov. J. Nucl. Phys. 28 (1978) 822.

[8] M. Derrick et al., ZEUS Collaboration, Phys. Lett. B345 (1995) 576.

[9] R.D. Ball, S. Forte, Phys. Lett. B335 (1994) 77.
R.D. Ball, S. Forte, Phys. Lett. B336 (1994) 77.

[10] I. Abt et al., H1 collaboration, DESY preprint DESY 93-103.

[11] G. Curci, W. Furmanski and R. Petronzio, Nucl. Phys. B175 (1980) 27;
W. Furmanski and R. Petronzio, Phys. Lett. B97 (1980) 437.

[12] W. Furmanski and R. Petronzio, Z. Phys. C11 (1982) 293.

[13] L.F. Abbott et al., Phys. Rev. D22 (1980) 582.
We extended a numerical program based on this reference to next-to-leading $\log(Q^2)$ according to the formalism given in [11].

[14] C. Pascaud and F. Zomer, LAL preprint LAL/94-42.

[15] W.J. Marciano, Phys. Rev. D29 (1984) 580.

[16] A.D. Martin, W.J. Stirling and R.G. Roberts, RAL preprint RAL-95-021.

[17] M. Glück, E. Hoffmann and E. Reya, Z. Phys. C13 (1982) 119.

[18] M. Glück, E. Reya and M. Stratmann, Nucl. Phys. B422 (1994) 37.

[19] E.Laenen et al., Nucl. Phys. B392 (1993) 162, 229;
E.Laenen et al., Phys. Letts. B291 (1992) 325;
S.Riemersma et al., Phys. Lett. B347 (1995) 143.

[20] T.Ahmed et al., H1 collaboration, Phys. Lett. B348 (1995) 681. submitted to Phys. Lett.

[21] J. Kwieciński, Z. Phys. C29 (1985) 561.

[22] D. Strozik-Kotlorz, Z. Phys. C53 (1992) 493.

[23] A.J. Askew et al., Phys. Rev. D49 (1994) 4042;
A.J. Askew et al., Mod. Phys. Lett. A8 (1993) 3813.

[24] P. Amaudruz et al., Phys. Lett. B295 (1992) 159;
CERN preprint CERN-PPE/92-124.

[25] A.C. Benvenuti et al., Phys. Lett. B223 (1989) 485;
CERN preprint CERN-EP/89-06.

[26] G. D'Agostini, Nucl. Instr. Meth. A346 (1994) 306.

[27] M. Virchaux and A. Milsztajn, Phys. Lett. B274 (1992) 221.

[28] CERN Program Library Long Writeup D506, CERN, Geneva 1993.

[29] Particle Data Group, Phys. Rev. D50 (1994) 1173.

[30] J.F. Owens, W.K. Tung, Ann. Rev. Nucl. Sci. 42 (1992) 291;
J. Botts et al., Phys. Lett. B304 (1993) 159;
H.L. Lai et al., Phys. Rev. D51 (1995) 4763.

[31] A.D. Martin, R.G. Roberts, W.J. Stirling, Phys. Rev. D47 (1993) 867;
A.D. Martin, R.G. Roberts, W.J. Stirling, Phys. Lett. B306(1993)145
and Erratum Phys. Lett. B309 (1993) 492;
A.D. Martin, R.G. Roberts, W.J. Stirling, Phys. Rev. D50 (1994) 6734.

[32] A.H. Mueller, Nucl. Phys. B (Proc. Suppl.) 18C (1990) 125.

[33] C. Pascaud and F. Zomer, LAL preprint LAL/95-05.

[34] K. Prytz, Phys. Lett. B311 (1993) 286.

[35] K. Prytz, Phys. Lett. B332 (1994) 393.

[36] R.K. Ellis, Z. Kunszt and E.M. Levin, Nucl. Phys. B420 (1994) 517.

[37] A.De Rujula, S.L.Glashow, H.D.Politzer, S.B.Treiman, F.Wilczek and A.Zee, Phys. Rev. D10(1974)1649;
A.Zee, F.Wilczek and S.B.Treiman, Phys. Rev. D10(1974)2881.

[38] R.D. Ball, S. Forte, CERN-TH.7421/94 and CERN-TH.7422/94.